We are IntechOpen,
the world's leading publisher of
Open Access books
Built by scientists, for scientists

6,900
Open access books available

186,000
International authors and editors

200M
Downloads

154
Countries delivered to

Our authors are among the

TOP 1%
most cited scientists

12.2%
Contributors from top 500 universities

CLARIVATE ANALYTICS
BOOK CITATION INDEX
INDEXED

WEB OF SCIENCE™

Selection of our books indexed in the Book Citation Index
in Web of Science™ Core Collection (BKCI)

Interested in publishing with us?
Contact book.department@intechopen.com

Numbers displayed above are based on latest data collected.
For more information visit www.intechopen.com

Quasi-3D Modeling of Sediment Transport for Coastal Morphodynamics

Yun-Chih Chiang and Sung-Shan Hsiao

Additional information is available at the end of the chapter

1. Introduction

Sand transport plays a very important role in many aspects of coastal and marine engineering. The balance of moving sands influences the construction of harbours, coastal defence, offshore wind turbine and oil rig, offshore platform and pipeline and many other engineering. Coastal sands may be carried by currents (such as tidal currents, wind-driven-currents, wave-driven-currents, storm surge driven currents), or by waves (monsoon waves or typhoon waves), or influenced by bedform changes, or all of them acting together and interacting in general sea state.

We can easily consider a sediment budget for a coastal area where a control section or a control volume is selected. The changing rate of net accretion or erosion of the coastal area of sea bed-level depends on the net transport rates at which sediments are entering or leaving the control section or the control volume. If the sum of the inflow sediment transport rates is larger than that of the outflows, the bed-level will tend to accrete; if the sum of the inflow sediment transport rates is smaller than that of outflow rates, the bedform will erode.

Consequently, accurate prediction of sediment transport rates is an important element in coastal engineering, foundations of offshore structures and morphological studies for the coastal environment. The procedure of the coastal morphological modeling system is shown as Fig. 1. The prediction of net sediment transport rates is a subject of great importance to coastal engineers and morphological modellers concerned with mediumand long-term shoreline changes. The aim of this chapter is to provide models for calculating the hydrodynamics and dynamic quantities of sediment transports in coastal zone, especially for the applications in surf zone.
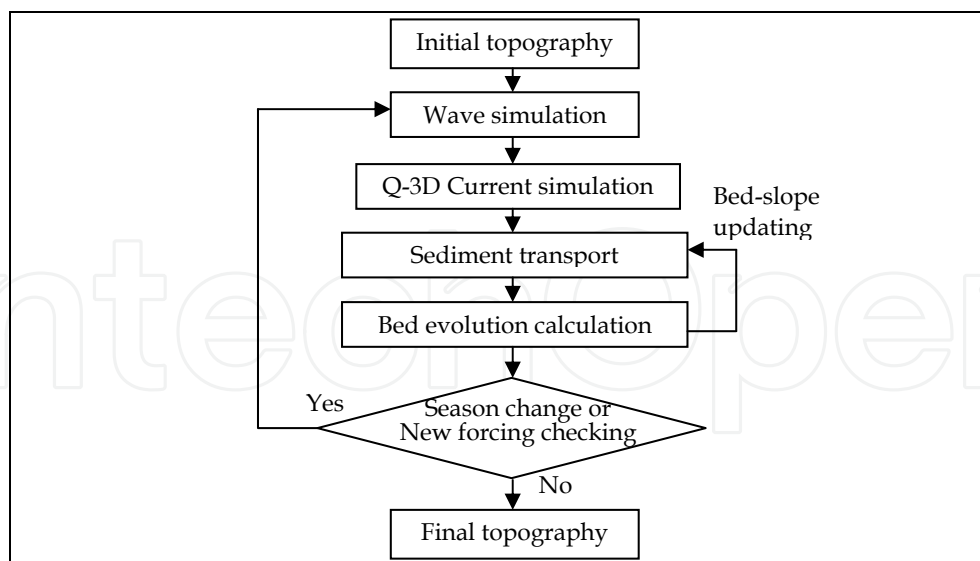
Figure 1. The procedure of the coastal morphological modeling system

1.1. Threshold of sediment motion

In order to estimate the changes of sediment budget, a quantitative evaluation of the net sediment transport rates are required. The sediment transport rate is defined as the amount of sediment per unit time entering or leaving a control volume, which is the vertical plane of unit width perpendicular to the sea mean water-level. The mechanics of sediment motion is depended on the effects of sediment dynamics while the frictions exerted on the sea bed by the hydrodynamics forcing agents, such as waves and currents.

While the friction exerted on the sea bed by waves and currents, the sediment 'entrainment' is the sand grains are carried up from bed. The 'bed load' sediment transport is the entraining sand grains rolling, hopping and sliding along the bedform, and is dominant with the inertial force and drag force on grains less than gravity force for slow flow or large grains. Suspended load sediment transport is the portion of the entraining sediment that is carried by the larger flow (or the wave large enough) which settles slowly enough and moves with the stream.

To estimate the sediment transport rate is more difficult, it may be divided into two components by cross-shore and longshore direction. The cross-shore sediment transport is mainly carried by the skewness and asymmetry wave orbital motion and cycle-mean water level around the surf zone. The longshore sediment transport is primarily dominated with wave-driven currents. In order to quantitate the sediment transport rate, included both bed load and suspended load, in each direction, an empirical relationship has been derived between 'transport rate' and the energetic-based components, such as bed shear-stress, wave-driven currents, wave orbit velocity….. and so on. The agreement between measurements (or experiments in hydraulic laboratory) and calculations associated with the relationship has been widely applied and predicts accurately sediment transport along long, straight-like beaches.

The total load sediment transport models are widely applied with coastal engineering in last three decades. Although the models are relatively simple and easy to use, but there are some weaknesses when applied around the surf zone. We will discuss in next section.

1.2. Interaction between sediment motion and bed features for morphodynamics

Nearshore sandbars are the important and popular feature of natural beaches morphodynamics. The cross-shore location of sandbars changes by the interactions between the sandbar and the sediment transport fluxes from waves and wave-driven-currents. Hoefel and Elgar (2003) indicated the mechanics of wave-induced sediment transport and sandbar migration: large waves breaking on the sandbars caused offshore mean currents, which maximum near the sandbar crest, will lead sandbars moved offshore; small waves pitching forward on the sandbars made the onshore acceleration skewness of wave orbital velocities, which maximum near the sandbar crest, will lead the sandbar moved onshore.

The nearshore sandbars could protect shorelines from wave attack by dissipating wave energy offshore through sandbar-crest-induced wave breaking. In general coasts, the dynamic behavior of nearshore sandbars are similar to quasi-cycle for storm and seasons waves alternated. However, the formation and evolution of sandbars are very important to coastal planners and engineers. Prediction of the dynamic behaviour of nearshore sandbar systems could be of great importance, there are many studies about the evolutions and migrations of nearshore sandbars by numerical simulations in last decade (Hsu et al., 2006; Long et al., 2006; Ruessink et al., 2007; Drønen and Deigaard, 2007; Houser and Greenwood, 2007; Ruessink and Kuriyama, 2008; Ruessink et al., 2009; Pape et al., 2010; Almar et al., 2010).
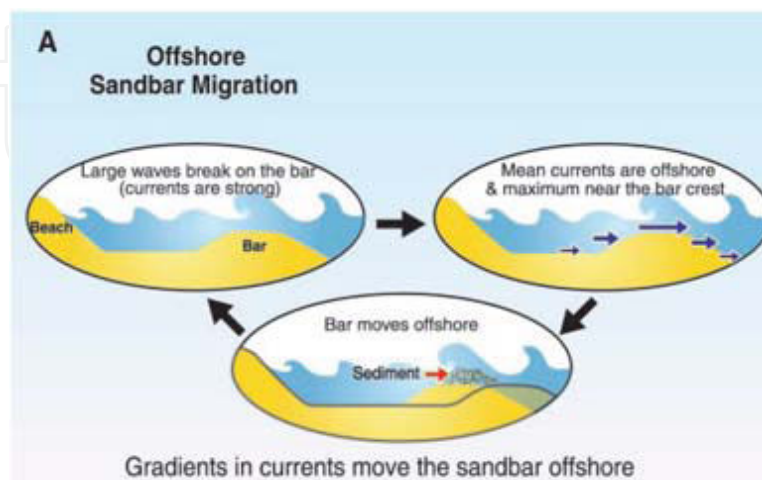

Figure 2. The mechanics of offshore sandbar migration. (Hoefel and Elgar,2003)
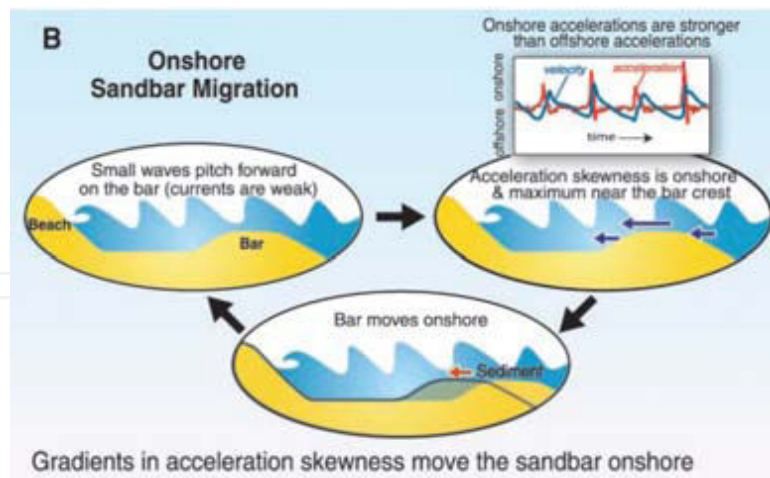
Figure 3. The mechanics of onshore sandbar migration. (Hoefel and Elgar,2003)

According to Hoefel and Elgar (2003), two mechanisms are commonly used in the explanation of morphodynamics of sandbars migration. The first mechanism type is the migration of offshore sandbars. The offshore sandbars migrated seaward observed during storms were driven primarily by a maximum in the offshore mean current (Under highly energetic storm conditions, breaking waves cause near bottom seaward flows, also called "undertow") near the sandbar crest. Offshore sandbar migration during storms results from feedback and interaction between breaking waves driven the "undertow" and bathymetric evolution (Elgar et al., 2001).

The second mechanism associates the migration of onshore sandbars. There are many studies have suggested mechanisms that could drive sandbars migration shoreward. Trowbridge and Young (1989) and Trowbridge and Madsen (1984) demonstrated that nonlinear wave boundary layer processes might play a role. Onshore sandbars migration might also be derived by the systematic changes in wave kinematics when passing over nearshore sandbars. As waves shoaling, their shapes are often described as "skewed" and "asymmetric" (Elgar, 1987), the mean water elevation depressed (the "Wave set-down") leads mean currents been weak. The non-breaking wave caused sediment transport over sandbars is driven predominately by wave asymmetric orbital velocities. Under the steep skewed and asymmetric waves, the water particle velocity is accelerated strongly as the asymmetric orbital velocity rapidly changes from maximum offshore to maximum onshore (e.g., Elgar et al., 1988).

In order to describe morphodynamics sandbars well, a key parameter for cross-shore sediment transport under breaking and near-breaking waves is well performed the near-bed skewed and asymmetric wave orbital velocity. Therefore, the three dimensionality of the hydrodynamic system should be considerable and must be taken into account. Most sediment transport models are based on phase-averaged wave models, depth-integrated hydraulic models (currents and wave driven currents) and sediment transport formula. In the hydraulic models, nearshore currents have previously been predicted by using two-dimensional models in the horizontal plane (2DH model). However, in the surf zone, the direction of current vectors

near the water surface is different from that at the sea-bottom because of the effect of undertow velocities. Nearshore currents have spiral profiles in the vertical direction. Undertows also play an important role in the morphodynamical changes on a littoral beach such as the cross-shore migration of longshore bars. In order to accurately predict the changes of sandbars migration, it is very important that the three-dimensional distribution of nearshore currents is determined. Therefore, well predicted nonlinear wave dynamics, vertical current and sediment transport models can be a good tool for nearshore sandbar morphodynamics, especially for cases where cross-shore transport mechanisms over sandbars are important. Drønen and Deigaard (2007) compared 2D horizontal depth-integrated approach and quasi-3D numerical model with formations of alongshore bars on gradual slope beach by normal and oblique incident waves, and the quasi-3D model produces a crescentic bar while the depth integrated model predicts almost straight sections of the bar interrupted by rip channels. Consequently, considering the accuracy and efficiency, a nonlinear waves model with quasi-3D sediment transport model can be applied as morphodynamics sandbar models.

1.3. The importance of quasi-3D sediment transport modeling

The numerical simulation of hydrodynamic and sediment transport processes form a powerful tool in the description and prediction of morphological changes and sediment budgets in the coastal zone. One of the key elements in a morphodynamics model is the correct quantification of local sand transport. Most sediment transport models are based on phase-averaged wave models, depth-integrated hydraulic models (currents and wave driven currents) and sediment transport formula. In the hydraulic models, nearshore currents have previously been predicted by using two-dimensional models in the horizontal plane (2DH model). However, in the surf zone, the direction of current vectors near the water surface is different from that at the sea-bottom because of the effect of undertow velocities. Nearshore currents have spiral profiles in the vertical direction. Undertows also play an important role in the morphological changes on a littoral beach such as the cross-shore migration of longshore bars. In order to accurately predict the changes of beach profile, it is very important that the three-dimensional distribution of nearshore currents is determined. Therefore, well predicted vertical current and sediment transport models can be a good tool for coastal area morphological modelling, especially for cases where cross-shore transport mechanisms are important. Considering the accuracy and efficiency, a quasi-3D model can be applied as a coastal profile model or a coastal area model.

Some models for determining the vertical distribution of nearshore currents have previously been proposed. de Vriend et al. (1987) presented a semi-analytical model and suggested that a 3D model is required when the sediment transport in the cross-shore direction becomes important; and then Svendsen and Lorenz (1989) proposed an analytical model composed of cross-shore and longshore current velocities. In recent years, many quasi-3D numerical models have been developed by extending 2DH model with one-dimensional velocity profile model defined in the vertical direction (1DV model), have also been proposed (Sanchez et al., 1992; Briand and Kamphuis, 1993; Okayasu et al., 1994; Elfrink et al., 1996; Rakha, 1998; Kuroiwa et al,. 1998; Drønen and Deigaard, 2000; Davis and Thorne, 2002; Fernando and Pan, 2005; Drønen and Deigaard, 2007; Li et al., 2007). In these models, the mean flow is determined by the 2DH

model, and the velocity profiles across water column in the vertical direction are resolved by using a 1DV model. While surface wave field and 3D flow field have been analyzed, sediment transport vectors in the horizontal plane can be calculated with the sediment transport profile across water column in the vertical direction.

The aim of this chapter is to develop an accurate model for estimation of local sediment transport rate of the nearshore both inside and outside of the surf zone. A two-dimensional 2D fully nonlinear Boussinesq wave module is combined with a quasi-3D hydrodynamic module (2DH and extended 1DV module). The 1DV hydrodynamic modules similar to those described by Elfrink et al. (1996) with surface-roller concept and a one-equation turbulence model are developed. The calculation of sediment transport rates is based on the formula with wave asymmetric and ripple-bed effects developed by Lin et al. (2009). The quasi-3D hydrodynamic modules are validated and compared, for regular waves over fixed beds. The local sediment transport rates is also calculated and validated with experimental data.

2. 2DH waves and nearshore currents models

In this section, the two-dimensional wave and nearshore current models are described as below:

2.1. Wave model

The wave model is based on the fully nonlinear Boussinesq equation developed by Wei et al. (1995); the equation is expressed by velocity with an arbitrary water depth. Bottom friction, wave breaking and subgrid lateral turbulent mixing as proposed by Kennedy et al. (2000), are also expressed by equations. The governing equations are shown as below:

$$\frac{\partial \eta}{\partial t} + \nabla \cdot [(h+\eta)u_\alpha] + \nabla \cdot \{(\frac{z_\alpha^2}{2} - \frac{h^2}{6})h\nabla(\nabla \cdot u_\alpha) + (z_\alpha + \frac{h}{2})h\nabla[\nabla \cdot (hu_\alpha)]\} = 0 \tag{1}$$

$$\frac{\partial u_\alpha}{\partial t} + g\nabla\eta + (u_\alpha \cdot \nabla u_\alpha) + z_\alpha\{\frac{z_\alpha}{2}\nabla(\nabla \cdot \frac{\partial u_\alpha}{\partial t}) + \nabla[\nabla \cdot (h\frac{\partial u_\alpha}{\partial t})]\} + R_f - R_b - R_s = 0 \tag{2}$$

In the above equations, $x=(x,y)$ are the horizontal coordinates coincident with the still water surface and z is the vertical coordinate; t is the time; ∇ is the horizontal gradient operator, defined as $(\partial/\partial x, \partial/\partial y)$; $\eta(x,t)$ is water surface elevation; g is the gravitational acceleration. $h=h(x)$ represents the water depth, $u_\alpha=(u_p,v_p)$ is the particle velocity vector at $z=z_\alpha$. R_f, R_b and R_s are the effects of bottom friction, wave breaking and subgrid lateral turbulent mixing, respectively. The detail mathematical operations are shown below,

$$R_f = \frac{K}{h+\eta} u_\alpha \mid u_\alpha \mid \tag{3}$$

K is the friction coefficient. The wave breaking term, $R_b = (R_{bx}, R_{by})$ is represented as

$$R_{bx} = \frac{1}{h+\eta}\{[\nu((h+\eta)u_\alpha)_x]_x + \frac{1}{2}[\nu((h+\eta)u_\alpha)_y \\ + \nu((h+\eta)v_\alpha)_x]_y\} \tag{4}$$

$$R_{by} = \frac{1}{h+\eta}\{[\nu((h+\eta)v_\alpha)_y]_y + \frac{1}{2}[\nu((h+\eta)u_\alpha)_y \\ + \nu((h+\eta)v_\alpha)_x]_x\} \tag{5}$$

The eddy viscosity (ν) is defined as

$$\nu = B\delta_b^2(h+\eta)\eta_t \tag{6}$$

Kennedy et al. (2000) proposed the mixing length, δ_b, is 1.2. The parameter B controls the occurrence of energy dissipation is defined as

$$B = \begin{cases} 1, & \eta_t \geq 2\eta_t^* \\ \dfrac{\eta_t}{\eta_t^*} - 1, & \eta_t^* < \eta_t \leq 2\eta_t^* \\ 0, & \eta_t \leq \eta_t^* \end{cases} \tag{7}$$

The onset and cessation of wave breaking using the parameter, η_t^*, is represented as

$$\eta_t^* = \begin{cases} \eta_t^{(F)}, & t - t_0 > T^* \\ \eta_t^{(I)} + \dfrac{t - t_0}{T^*}(\eta_t^{(F)} - \eta_t^{(I)}), & 0 \leq t - t_0 < T^* \end{cases} \tag{8}$$

$$\eta_t^{(I)} = 0.65\sqrt{gh}, \eta_t^{(F)} = 0.15\sqrt{gh}, T^* = 5\sqrt{h/g} \tag{9}$$

where T^* is the transition time, t_0 is the time when wave breaking occurs, and t-t_0 is the age of the breaking event. The subgrid lateral mixing terms $R_s = (R_{sx}, R_{sy})$ is displayed as follow

$$R_{sx} = \frac{1}{h+\eta}\{[v_s((h+\eta)u_\alpha)_x]_x + \frac{1}{2}[v_s((h+\eta)u_\alpha)_y + v_s((h+\eta)v_\alpha)_x]_y\} \tag{10}$$

$$R_{sy} = \frac{1}{h+\eta}\{[v_s((h+\eta)v_\alpha)_y]_y + \frac{1}{2}[v_s((h+\eta)u_\alpha)_y + v_s((h+\eta)v_\alpha)_x]_x\} \tag{11}$$

The parameter v_s is the eddy viscosity due to the subgrid turbulence.It can be calculated by:

$$v_s = c_m \Delta x \Delta y [(U_x)^2 + (V_y)^2 + \frac{1}{2}(U_y + V_x)^2]^{1/2} \tag{12}$$

where c_m is the mixed coefficient.

2.2. 2DH nearshore current model

Based on computed characteristics of wave fields, the radiation stress terms can then be found and input into the depth integrated (2DH) nearshore current module, which solves the depth-and-wave-period averaged continuity and momentum equations at each local point on horizontal plane, for calculating wave driven current:

$$\frac{\partial \eta}{\partial t} + \frac{\partial}{\partial x}[U(h+\eta)] + \frac{\partial}{\partial y}[V(h+\eta)=0] \tag{13}$$

$$\frac{\partial U}{\partial t} + U\frac{\partial U}{\partial x} + V\frac{\partial U}{\partial y} = fV - g\frac{\partial \eta}{\partial x} + \frac{1}{\rho}\left(\frac{\partial \tau_{xx}}{\partial x} + \frac{\partial \tau_{yx}}{\partial y}\right) + \frac{1}{\rho(h+\eta)}(\tau_{sx} - \tau_{bx}) - \frac{1}{\rho(h+\eta)}\left(\frac{\partial S_{xx}}{\partial x} + \frac{\partial S_{yx}}{\partial y}\right) \tag{14}$$

$$\frac{\partial V}{\partial t} + U\frac{\partial V}{\partial x} + V\frac{\partial V}{\partial y} = -fV - g\frac{\partial \eta}{\partial y} + \frac{1}{\rho}\left(\frac{\partial \tau_{xy}}{\partial x} + \frac{\partial \tau_{yy}}{\partial y}\right) + \frac{1}{\rho(h+\eta)}(\tau_{sy} - \tau_{by}) - \frac{1}{\rho(h+\eta)}\left(\frac{\partial S_{xy}}{\partial x} + \frac{\partial S_{yy}}{\partial y}\right) \tag{15}$$

where U and V are depth-integrated nearshore current velocities in x and y direction respectively, S_{xx}, S_{xy} and S_{yy} are radiation stress tensor, g is acceleration due to gravity, ϱ is water density, h is water depth, η is water surface elevation, τ_{xx}, τ_{xy} and τ_{yy} are Reynolds stress tensor, τ_s and τ_b are shear stress on surface and bottom. The friction factor for combined wave-current flow in bottom shear stresses and the mixing coefficient in Reynolds stresses are suggested by Chiang et al. (2010).

3. Quasi-3D extended: 1DV velocity model

Fig. 4 depicts the coordination of the quasi-3D hydraulic system. The x coordinate is defined in the cross-shore direction towards shore. The y coordinate denotes the long shore direction. The Z coordinate is toward from sea bed to surface in depth-direction.

3.1. Numerical formulation

The distributions of the velocity profiles in the long-shore and cross-shore direction at each local point along the vertical water column are found through the following momentum equations:

$$\frac{\partial u}{\partial t} = -\frac{1}{\rho}\frac{\partial p}{\partial x} + \frac{\partial}{\partial z}\left(\nu_t \frac{\partial u}{\partial z}\right) + \frac{1}{\rho}\frac{\partial \overline{\tau^x}}{\partial z} \tag{16}$$

$$\frac{\partial v}{\partial t} = -\frac{1}{\rho}\frac{\partial p}{\partial y} + \frac{\partial}{\partial z}\left(\nu_t \frac{\partial v}{\partial z}\right) + \frac{1}{\rho}\frac{\partial \overline{\tau^y}}{\partial z} \tag{17}$$

where u and v are wave-period-averaged velocities across the water column in the cross-shore and long-shore direction respectively, p is the pressure, ν_t is the turbulence viscosity, $\overline{\tau^x}$ and $\overline{\tau^y}$ are wave-period-averaged wave-induced shear stress through water column. In equation (16) and (17), the convection terms in the left hand side of the equations have been neglected which follows the conventional 1DV type of models by assuming the spatial gradient at the interested site is small. This is due to the fact that the convection terms have been counted in the 2DH nearshore current model and the 1DV model is only used to resolve the vertical profile of the flow velocities and sediment concentration in suspension.
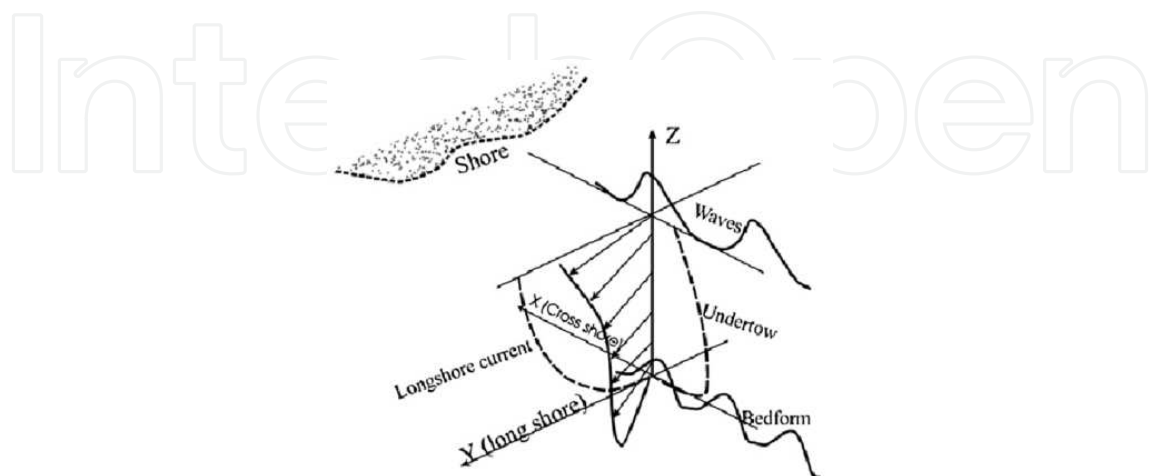

Figure 4. The coordination of the quasi-3D hydraulic system

The pressure gradient term may be divided into two components by inside/outside boundary layer. The pressure gradient term can be easily calculated from the variation of cycle-mean water free surface. Within the boundary layer, we can calculate from the time differential of velocity at boundary layer:

$$\frac{\partial p}{\partial x} = \frac{dU_{w0}^{x}}{dt}, \frac{\partial p}{\partial y} = \frac{dU_{w0}^{y}}{dt} \tag{18}$$

where U_{w0}^{x} and U_{w0}^{y} is the wave orbit velocity outside the boundary layer.

The cycle-mean wave-induced shear stress under waves is consist of wave motion component (τ_w), wave breaking surface roller component (τ_r), boundary layer streaming component (τ_b) and mean water surface changed (wave set-up/set-down) component (τ_{su}), as shown in Fig. 5. The Boundary layer streaming components can be neglected, because it is small than the others. The total shear stress is defined as

$$\overline{\tau} = \tau_w + \tau_r + \tau_{su} \tag{19}$$

The shear stress distribution due to wave motion (τ_w) is in accordance with the derivations of Deigaard and Fredsoe (1989):

$$\tau_w = \frac{-1}{c}\frac{dE_f}{dx}\left(1 + \frac{h-y}{2h}\right) \tag{20}$$

where E_f is cycle-mean energy flux due to wave motion (Svendsen, 1984):

$$E_f = \rho gc\overline{\eta}^2 = B\rho gcH^2 \tag{21}$$

The coefficient B is 1/12 while wave breaking and 1/8 in general.

The shear stress due to wave breaking (τ_w) can be calculated by the concept of surface roller. According to Svendsen (1984) and Deigaard et al. (1986), the shear stress of surface roller is assumed to be constant by experiment:

$$\tau_r = -\frac{\rho}{T}\frac{d(Ac)}{dx} \tag{22}$$

where c is wave celerity, T is wave period, and A is the area of surface roller (as shown in Fig. 7) can be easily calculated by $A=0.09H$ (Deigaard et al., 1986).
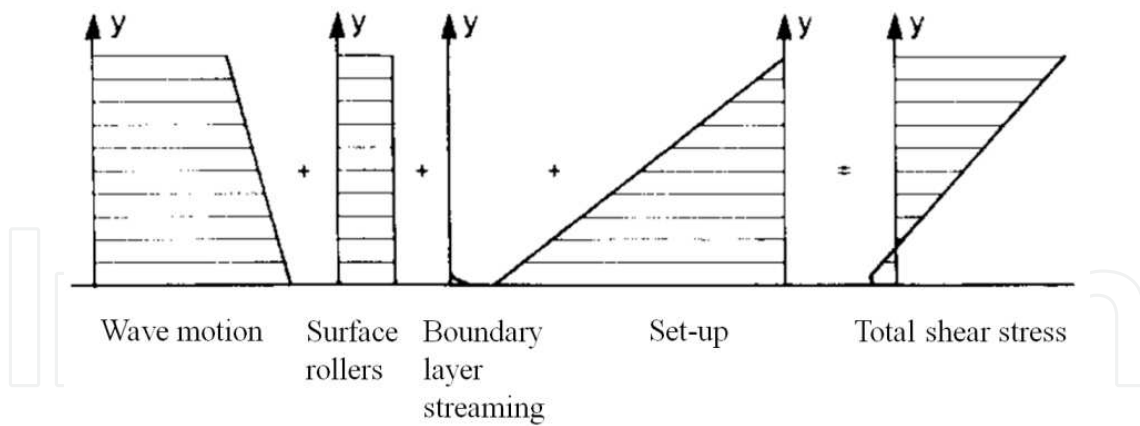
Figure 5. Total shear stress and its component from surface to bed in vertical direction under wave

The shear stress due to variation of mean water level (τ_{su}) can be easily calculated by

$$\tau_{su} = -\rho g h \left(1 - \frac{z}{h}\right) \frac{\partial \overline{\eta}}{\partial x} \tag{23}$$

The turbulence viscosity should be specified through certain turbulence models. In the present study, the one-equation k-closure is adopted as follows:

$$\frac{\partial k}{\partial t} = \frac{\partial}{\partial z}\left(\frac{\nu_{tb}}{\sigma_k} \frac{\partial k}{\partial z}\right) + \nu_{tb}\left[\left(\frac{\partial u}{\partial z}\right)^2 + \left(\frac{\partial v}{\partial z}\right)^2\right] + \frac{P_r}{\rho} - \varepsilon \tag{24}$$

where k is the turbulent kinetic energy, constant σ_k=1.0, P_r is the turbulent production due to surface wave breaking by surface-roller concept and ε is dissipation rates which is given as:

$$\varepsilon = c_1 k^{3/2} / l \tag{25}$$

in which l is the turbulence length scale computed as (Deigaard et al., 1991):

$$l = \begin{cases} c_1^{1/4}\kappa z & ,z \leq l_{max} / \left(\kappa c_1^{1/4}\right) \\ l_{max} & ,z > l_{max} / \left(\kappa c_1^{1/4}\right) \end{cases} \tag{26}$$
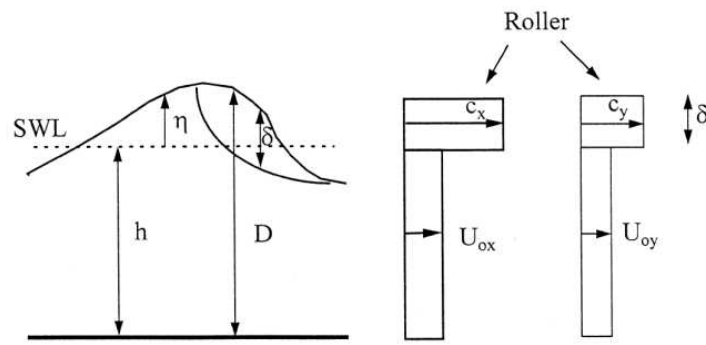
where l_{max}=0.1h, c_1=0.09.

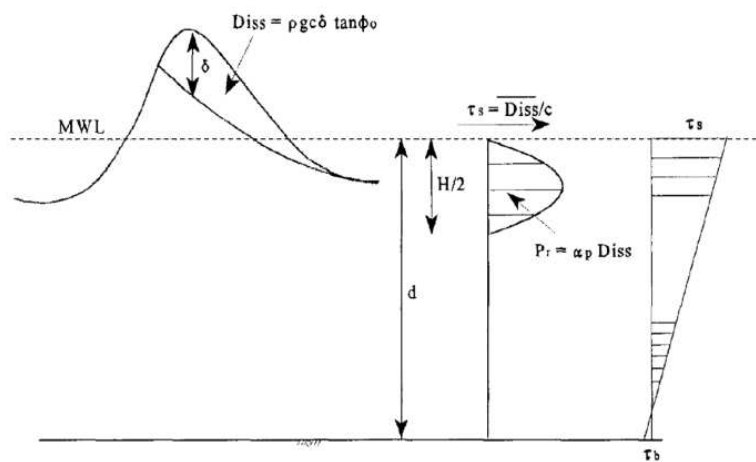**Figure 6.** The concept of surface roller due to wave breaking (Deigaard et al., 1986)

Figure 7. The turbulence generated and energy dissipation due to wave breaking (Deigaard et al., 1986)

The turbulence generated and energy dissipation at the water surface due to wave breaking is computed following Deigaard et al. (1991), as shown in Fig. 7 :

$$P_r = \alpha_p \text{DISS} \tag{27}$$

where constant α_p = 0.33, the energy dissipation term DISS is suggested by Deigaard (1989):

$$\text{DISS} = \rho g c \delta_r \tan \phi_0 \tag{28}$$

where c is wave celerity, φ_0 is wave initial breaking angle as 10 degree, δ_r is thickness of surface roller head suggested by Deigaard et al. (1986):

$$\delta_r = \frac{2(h + H/2)}{L} \tag{29}$$

3.2. Boundary condition and key parameters

3.2.1. Eddy viscosity

According to Brøker et al. (1991), the eddy viscosity is calculated by assuming the total kinetic energy could be the sum of three contributions: the oscillatory near bed boundary layer (v_{tw}), wave breaking (v_{tb}), and the time-averaged currents (v_{tU}) respectively. The eddy viscosity outside and inside the wave boundary layer is calculated by eq. (30), and eq. (31).

$$v_t = \sqrt{v_{tU}^2 + v_{tb}^2} \tag{30}$$

$$v_t = \sqrt{v_{tw}^2 + v_{tb}^2} \tag{31}$$

The component of oscillatory near bed boundary layer (v_{tw}) is calculated from (Okayasu et al., 1988)

$$v_{tw} = z\kappa U_f \tag{32}$$

where $\kappa=0.4$ is von karman constant, $U_f = \sqrt{\tau_b/\rho}$ is the frictional velocity under wave.

The component of wave breaking (v_{tb}) is calculated from (Rakha, 1998):

$$v_{tb} = l\sqrt{k} \tag{33}$$

where k is turbulence kinetic energy, and l is turbulence length scale.

The contribution of the time-averaged currents (v_{tU}) is calculated also from (Rakha, 1998):

$$v_{tU} = l_{max}^2 \sqrt{\left(\frac{du}{dz}\right)^2 + \left(\frac{dv}{dz}\right)^2} \tag{34}$$

where l_{max} is the same as eq. (26).

3.2.2. Thickness of wave boundary layer

The thickness of wave boundary layer (δ_w) is calculated from (Soulsby et al., 1993):

$$\delta_w = \frac{u_{*\max}T}{2\pi} \tag{35}$$

where $u_{*\max} = \sqrt{\tau_{\max}/\rho}$, $\tau_{\max}$ is the maximum shear stress by waves and currents.

4. Sediment transport formula

The total sediment transport is consisted of bed load and suspended load suggested by Chiang et al. (2011):

$$q_{total} = q_b + q_s \tag{36}$$

where q_b is the bed load sediment transport rate, and the q_s is the suspended load sediment transport rate.

4.1. Bed load sediment transport

Following Chiang et al. (2011), the instantaneous bed load transport rate due to wave asymmetric and ripple-bed effects is given as:

$$q_b = \overline{\Phi_b}\left[g(s-1)d_{50}^3\right]^{1/2} \tag{37}$$

$$\overline{\Phi_b} = \left(\overline{\Phi_{bx}}^2 + \overline{\Phi_{by}}^2\right)^{1/2} \tag{38}$$

$$\overline{\Phi_{bx}} = 11\left[t_c\left(\theta_{cx}-\theta_c\right)^{1.65} - t_t\left(\theta_{tx}-\theta_c\right)^{1.65}\right] \tag{39}$$

$$\overline{\Phi_{by}} = 11\left(\theta_y-\theta_c\right)^{1.65} \tag{40}$$

where g being the gravity acceleration, s the relative density ($s=\rho_s/\rho$, with ρ_s the density of sediment), d_{50} is median diameter, Φ_b is dimensionless sediment transport rates, subscript x, y indicates along wave propagating and perpendicular direction. The wave-crest-half period, wave-trough-half period, and perpendicular wave-period averaged equivalent Shields stress are suggested by Chiang et al. (2011) as following:

$$\theta_{cx} = \frac{1}{2} \frac{\left(f_{cw}\right)_{cx} u_{cx}^2}{(s-1)g d_{50}} \tag{41}$$

$$\theta_{tx} = \frac{1}{2} \frac{\left(f_{cw}\right)_{tx} u_{tx}^2}{(s-1)g d_{50}} \tag{42}$$

$$\theta_y = \frac{1}{2} \frac{f_c U_0^2 \sin^2(\phi)}{(s-1)g d_{50}} \tag{43}$$

where f_w, f_c, and f_{cw} are the friction coefficient of wave, current and wave-current interaction, u_{cx} and u_{tx} are equivalent phase-averaged near-bed velocity under crest and trough half period.

$$f_w = \begin{cases} 0.00251 \times \exp\left[5.21 \times \exp\left(\dfrac{a_w}{K_s}\right)^{-0.19}\right], & \dfrac{a_w}{K_s} > 1.57 \\ 0.3, & \dfrac{a_w}{K_s} \le 1.57 \end{cases} \tag{44}$$

$$f_c = 2\left[\frac{0.4}{\ln(h/z_0)-1}\right]^2 \tag{45}$$

$$\left(f_{cw}\right)_i = \varepsilon_i f_c + (1-\varepsilon_i) f_{wi} \tag{46}$$

where $i = c$(crest) or t(trough), and weigh coefficient given as:

$$\varepsilon_c = \frac{U_0}{U_{w\max} + U_0} \tag{47}$$

$$\varepsilon_t = \frac{U_0}{\left|U_{w\min}\right| + U_0} \tag{48}$$

In eq. (44), a_w is half wave orbit closure:

$$a_w = \frac{U_w T}{2\pi} \tag{49}$$

According to Soulsby (1997), the total roughness (K_s) of sea bed during wave passing is consisted of grain related component (K_{ss}), form drag component (K_{sf}) and sediment transport component (K_{st}):

$$K_s = K_{ss} + K_{sf} + K_{st} \tag{50}$$

In eq. (37), the grain related component is given as (Nielson, 1992 and Soulsby, 1997),

$$K_{ss} = 2.5 \times d_{50} \tag{51}$$

The form drag component associated with sandy ripples is defined (Davis and Villaret, 2003):

$$K_{sf} = 25\eta_r \left(\eta_r / \lambda_r \right) \tag{52}$$

where the λ_r and η_r is the wave length and wave height of full-developped sandy ripples, the empirical relationship formula is shown as Nielson (1992). The sediment transport component of friction roughness (K_{st}) is given as (Wilson, 1989):

$$K_{st} = 5\theta_s d_{50} \tag{53}$$

In eq. (40), d_{50} is the sediment median grain size, and θ_s is the entraining bed shear-stress.

4.2. Suspended load sediment transport

The suspended sediment transport can be calculated by integrated sediment concentration (C) of vertical water column from bottom to surface. The sediment concentration C in the water column is found through the mass conservation equation:

$$\frac{\partial C}{\partial t} = w_s \frac{\partial C}{\partial z} + \frac{\partial}{\partial z}\left(\varepsilon_{sd} \frac{\partial C}{\partial z} \right) \tag{54}$$

where w_s is settling velocity, ε_{sd} is the coefficient of sediment diffusion. According to Fredsøe and Deigaard (1992), ε_{sd} is equivalent to turbulent eddy viscosity ν_t. The settling velocity is defined as (Soulsby, 1997):

$$w_s = \frac{\nu}{d_{50}}\left[\left(10.36^2 + 1.049D_*^3\right)^{1/2} - 10.36 \right] \tag{55}$$

where D_* is the dimensionless grain diameter:

$$D_* = \left[\frac{g(s-1)}{v^2} \right]^{1/3} d_{50} \tag{56}$$

After the suspended sediment concentration and vertical velocity profiles obtained, the instantaneous suspended transport rate can be evaluated as:

$$q_s = \int_{z_a}^{h} \overline{c}(z)\overline{u}(z)dz \tag{57}$$

where z_a is the The reference height a is specified as $2.5d_{50}$ (Soulsby, 1997), h is the water depth.

5. Model validation and discussion

The quasi-3D sediment tranport model is validated against wave flume tests and existed numerical models.

5.1. Model validation with Cox and Kobayashi (1996)

The wave and quasi-3D model system described above was firstly tested by regular wave with uniform sloped bed, and compared with experiment (Cox and Kobayashi, 1996). The test conditions are given: wave height 13.2cm, wave period 2.2 sec, the length of wave flume is 14.0m, width is 1.5m, depth is 30.0cm, slope-1:35; sand medium diameter is 1.0mm, and bed roughness height k_s=1mm. The numerical results of wave height and layouts of wave flume is shown as Fig. 8. In Fig. 8, the black triangles indicate experimental data by Cox and Kobayashi (1996), the red line is the results of present wave model, and the black line is the numerical results from Rakha (1998). The wave nonlinear effects and wave breaking and regenerating can be observed well, it's shown good agreement with experiment.
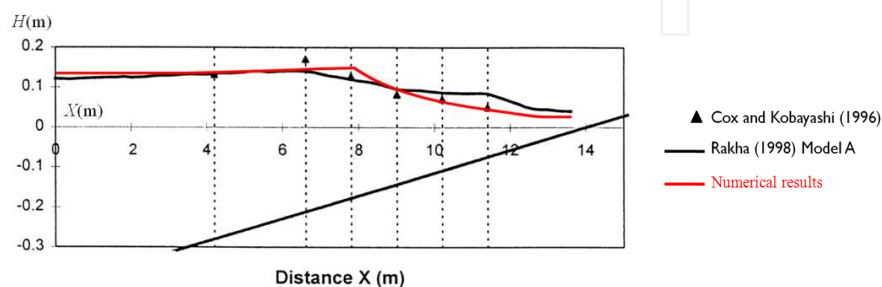

Figure 8. The validation of wave height and the layout of wave flume with results from Cox and Kobayashi (1996)

The comparisons of the vertical velocity profile at various position used by Cox and Kobayashi (1996) are also adopted here to assess the present model's accuracy for wave propagating at a slope in wave flume. The velocity profiles of various position are shown as Fig. 9 ~ Fig. 14. The black triangles also indicate experimental data by Cox and Kobayashi (1996), the blue line is the results of present 1DV model, and the black line is the numerical results from Rakha (1998). Compared with experiments, they are shown good performance for the validation of distribution of the vertical velocity profile before and after wave breaking.
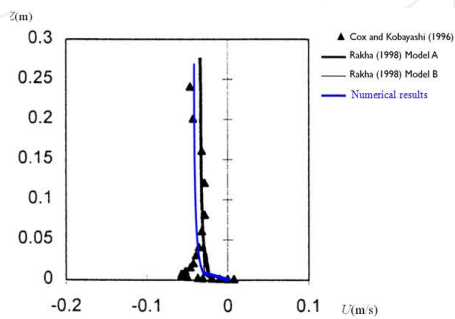

Figure 9. The validation of vertical velocity profile at wave flume x=4.2m from Cox and Kobayashi (1996)
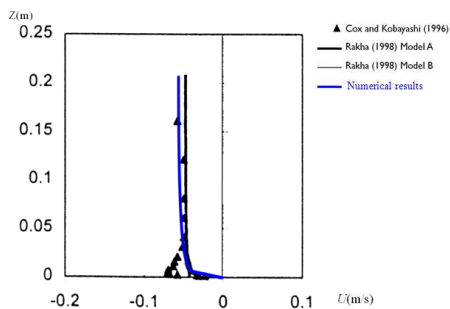

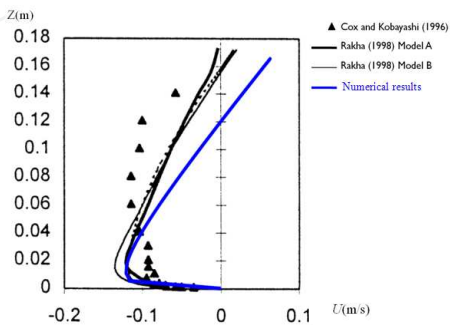**Figure 10.** The validation of vertical velocity profile at wave flume x= 6.6m from Cox and Kobayashi (1996)

Figure 11. The validation of vertical velocity profile at wave flume x=7.8m from Cox and Kobayashi (1996)
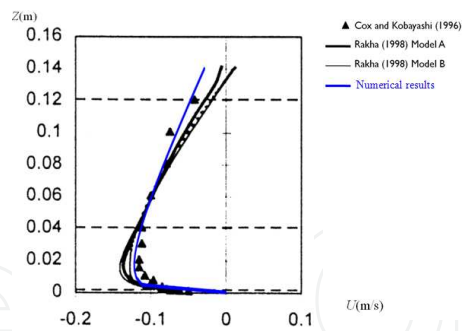
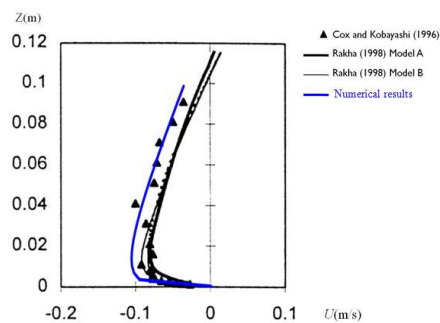**Figure 12.** The validation of vertical velocity profile at wave flume x= 9.0m from Cox and Kobayashi (1996)

Figure 13. The validation of vertical velocity profile at wave flume x= 10.2m from Cox and Kobayashi (1996)
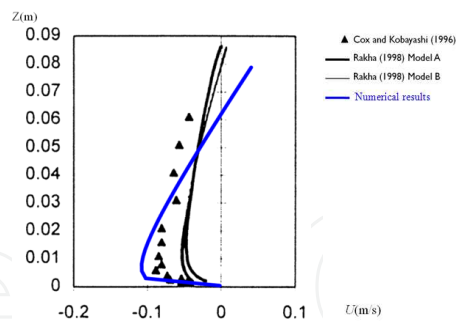

Figure 14. The validation of vertical velocity profile at wave flume x= 11.4m from Cox and Kobayashi (1996)

5.2. Model validation with Ting and Kirby (1994)

The Boussinesq wave model and quasi-3D nearshore current model system described above was tested by regular wave with uniform sloped bed, and compared with experiment (Ting and Kirby, 1994, test 1). The test conditions are given: wave height 12.5cm, wave period 2.0 sec, the length of wave flume is 13.0m, width is 1.5m, depth is 30.0cm, slope-1:35; sand medium diameter is 1.0mm, and bed roughness height ks=1mm. The numerical results of wave height and layouts of wave flume is shown as Fig. 15. In Fig. 15, the black triangles indicate

experimental data by Ting and Kirby (1994), the red line is the results of present wave model, and the black line is the numerical results from Rakha (1998). The wave nonlinear effects and wave breaking and regenerating can be observed well, it's also shown good agreement with experiments.
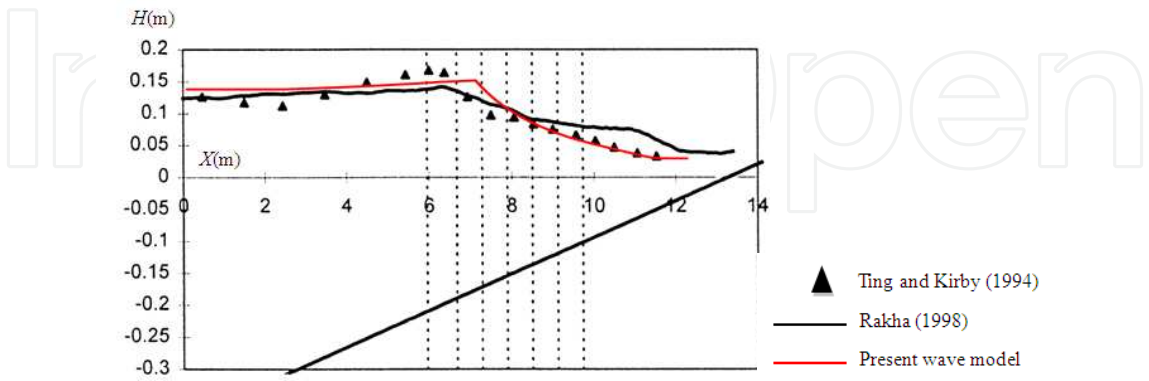

Figure 15. The validation of wave height and the layout of wave flume with results from Ting and Kirby (1994), test 1

The comparisons of the vertical velocity profile at various position used by Ting and Kirby (1994) are also adopted here to assess the present model's accuracy for wave propagating at a slope in wave flume. The velocity profiles of various position are shown as Fig. 16 ~ Fig. 21. The black triangles also indicate experimental data by Ting and Kirby (1994), the blue line is the results of present 1DV model, and the black line and dotted line are the numerical results from Rakha (1998) model A and model B. Compared with experiments, they are shown good performance for the validation of distribution of the vertical velocity profile before and after wave breaking. Because of full-nonlinear Bossinesq wave model and accuracy wave breaking dissipation terms in 1DV model, the present model performed well than Rakha (1998).

5.3. Validation for sediment transport calculations

To assess the present quasi-3D sediment transport model's ability of prediction for local sediment transport under combined waves and currents for a range conditions, a series of
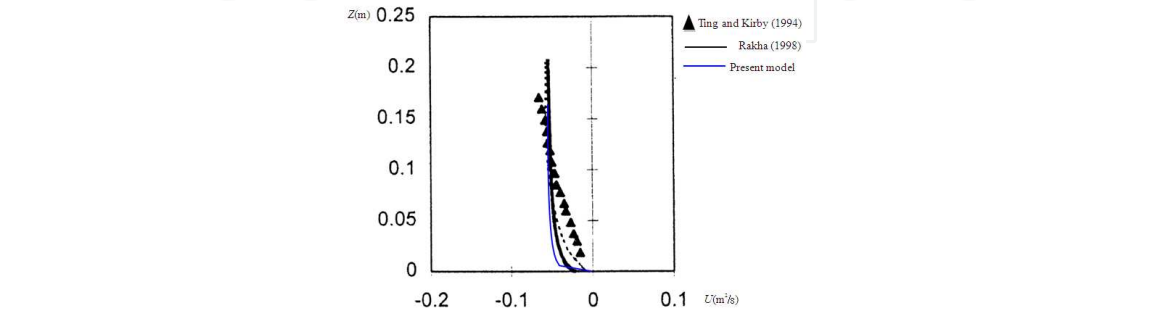

Figure 16. The validation of vertical velocity profile at wave flume x=5.945m with results from Ting and Kirby (1994)
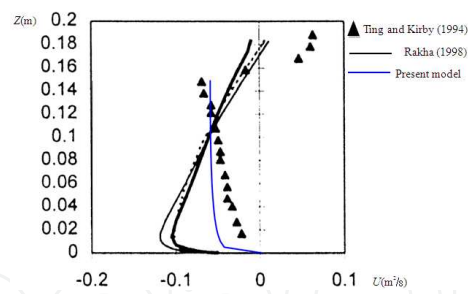
Figure 17. The validation of vertical velocity profile at wave flume x=6.665m with results from Ting and Kirby (1994)

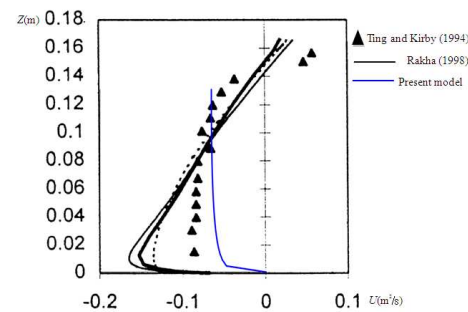**Figure 18.** The validation of vertical velocity profile at wave flume x=7.275m with results from Ting and Kirby (1994)

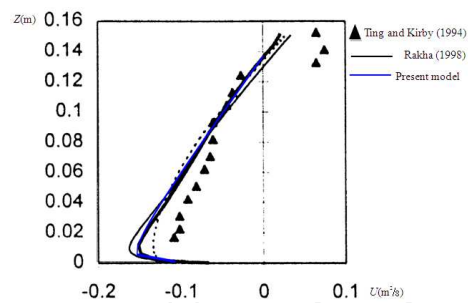
Figure 19. The validation of vertical velocity profile at wave flume x=7.885m with results from Ting and Kirby (1994)
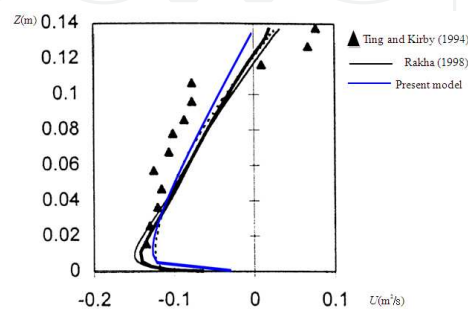

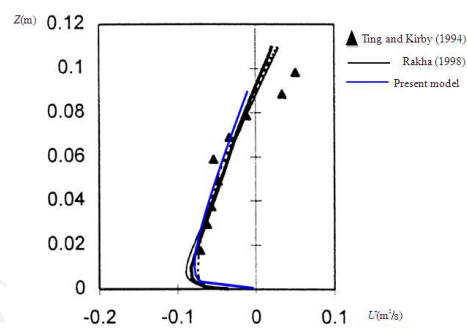**Figure 20.** The validation of vertical velocity profile at wave flume x=8.495m with results from Ting and Kirby (1994)

Figure 21. The validation of vertical velocity profile at wave flume x=9.110m with results from Ting and Kirby (1994)

experiments in the wave flume have been observed by Dibajnia and Watanabe (1998), Dibajnia and Kioka (2000), and Dibajnia et al. (2001). All of experimental data are shown as Table 1.

The comparison has been carried out between the period-averaged net sediment transport and experimental results for different wave-current conditions and the results are reasonable accurate within a factor of 2, as shown in Fig. 22. There are 66% numerical results greater than experiments, and 8% numerical results out of compared accurate factor of 2. They are shown good performance to predict the local sediment transport rates in nearshore region.

$D_{50}(cm)$	$2U_w(cm/s)$	$T(sec)$	$u_{max}/2U_w$	$2T_{pc}/T$	$U_0(cm/s)$	$q(cm^2/s)$
0.02	163.8	3.9	0.67	0.29	0	0.133
0.02	148.2	3.9	0.68	0.29	0	0.094
0.02	136.1	3.9	0.68	0.29	0	0.079
0.02	126.9	3.9	0.67	0.29	0	0.042
0.02	103.9	3.7	0.59	0.41	0	0.014
0.02	119.4	3.7	0.59	0.41	0	0.055
0.02	128.5	3.7	0.59	0.41	0	0.048
0.02	136.5	3.8	0.58	0.42	0	0.051
0.02	140.5	3.5	0.68	0.32	0	0.08
0.02	129	3.5	0.68	0.32	0	0.049
0.02	121.2	3.6	0.68	0.31	0	0.061
0.02	108.4	3.6	0.6	0.39	0	0.031
0.02	144.8	3.8	0.58	0.42	0	0.072
0.02	122.8	3.6	0.68	0.31	0	0.041
0.02	117.1	3.5	0.59	0.41	0	0.032
0.02	119.8	3.5	0.59	0.41	0	0.046
0.02	114.6	3.6	0.60	0.4	0	0.044
0.02	109.5	3.9	0.67	0.29	0	0.062

D_{50}(cm)	$2U_w$(cm/s)	T(sec)	u_{max}/$2U_w$	$2T_{pc}$/T	U_0(cm/s)	q(cm²/s)
0.02	126.3	3.5	0.59	0.41	0	0.032
0.02	105.6	3.6	0.68	0.31	0	0.043
0.02	137.3	3.5	0.67	0.33	0	0.086
0.02	122.9	3.9	0.67	0.29	0	0.066
0.02	112.7	3.7	0.59	0.41	0	0.046
0.02	135.9	3.5	0.59	0.41	0	0.069
0.02	119.2	3.9	0.68	0.3	16.3	0.117
0.02	114.7	3.8	0.58	0.42	14.3	0.095
0.02	116.1	3.7	0.59	0.41	5.6	0.063
0.02	118.8	3.9	0.68	0.29	11	0.1
0.02	189.5	4	0.65	0.31	0	0.21
0.02	184.2	3.8	0.64	0.35	0	0.171
0.02	167.5	3.8	0.65	0.33	0	0.134
0.02	151.7	3.8	0.67	0.31	0	0.109
0.02	183.2	3.6	0.65	0.34	0	0.142
0.02	183.2	3.6	0.65	0.35	0	0.139
0.02	179.3	3.6	0.65	0.34	0	0.123
0.02	175.6	3.6	0.65	0.34	0	0.103
0.02	165.5	3.6	0.65	0.33	0	0.125
0.02	163.4	3.6	0.65	0.34	0	0.119
0.02	155.6	3.6	0.66	0.33	0	0.082
0.02	146.4	3.6	0.65	0.33	0	0.075
0.055	275.3	4.2	0.57	0.43	0	1.184
0.055	265	4.1	0.59	0.41	0	0.773
0.055	239.1	4	0.62	0.37	0	0.683
0.055	208.3	4	0.64	0.36	0	0.439
0.055	264.8	3.6	0.59	0.41	0	0.634
0.055	260.1	3.6	0.61	0.39	0	0.534
0.055	250.1	3.6	0.62	0.38	0	0.56
0.055	225.3	3.6	0.63	0.37	0	0.459
0.08	280.5	4.2	0.57	0.43	0	1.373
0.08	276.3	4.1	0.57	0.43	0	1.44
0.08	270.2	3.6	0.57	0.43	0	1.137
0.08	264.2	4	0.58	0.42	0	0.8

Table 1. Experiments from Dibajnia and Watanabe (1998), Dibajnia and Kioka(2000), and Dibajnia et al. (2001).
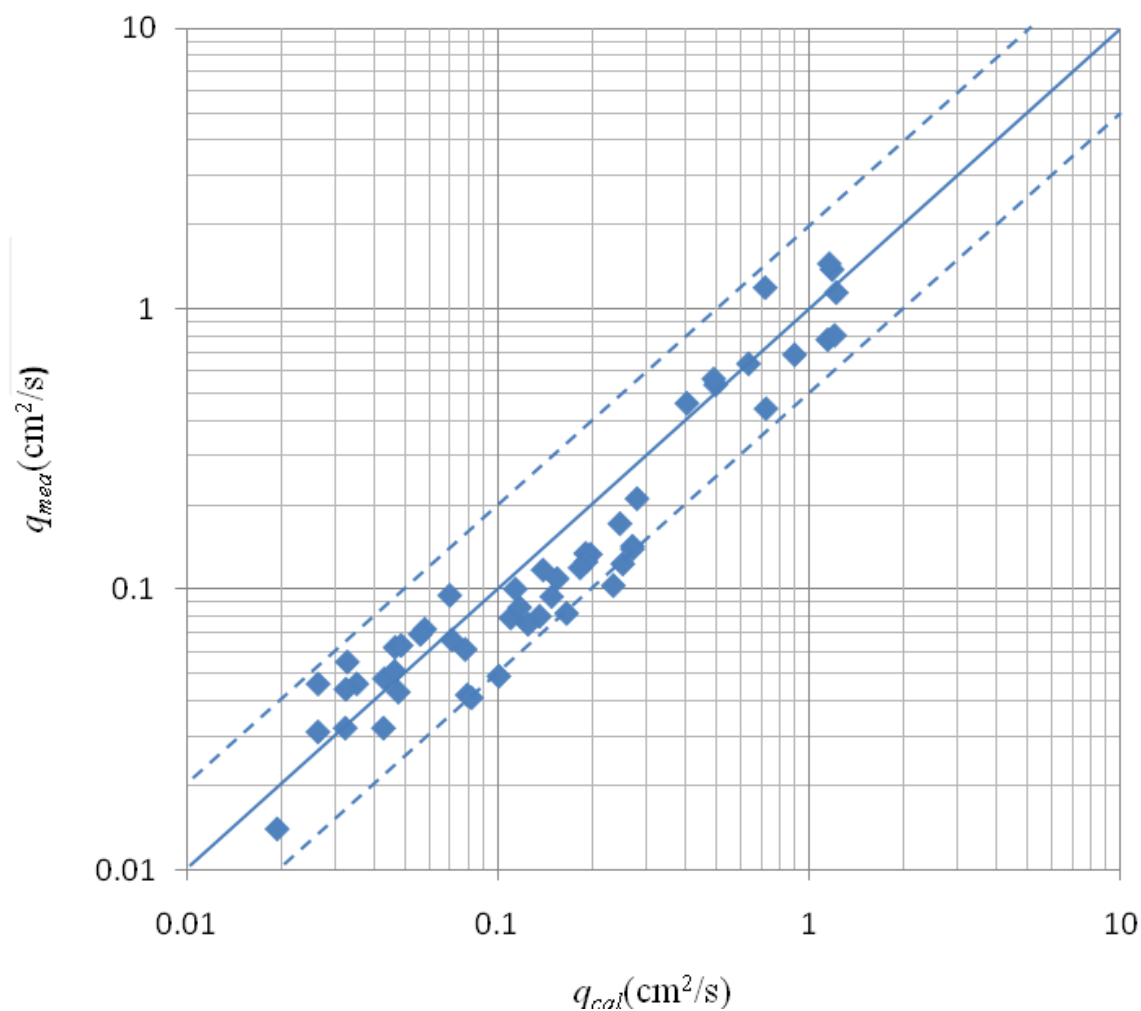
Figure 22. Measured against calculated sediment transport rates with present model and experimental results from Dibajnia and Watanabe (1998), Dibajnia and Kioka(2000), and Dibajnia et al. (2001).

6. Conclusion

In this chapter, a quasi-3D numerical model has been developed to predict sand transport in the coastal region. The whole model system is consisted of a fully nonlinear Bossinesq wave module, 2HD depth-integral wave-driven current module, 1DV velocity profile module, and the sediment transport formula. Numerical results indicate that the wave breaking and regenerating are good agreement with experiments. The phenomenon of undertow for wave breaking or not is performed well, and the vertical velocity profiles are shown good accuracy with experiments. The numerical results of sediment transport have been compared with experiment and obtained are reasonably accurate within a factor of 2. The quasi-3D sediment transport model system was then used to simulate several laboratory studies to test its ability to reproduce the important nearshore morphodynamic processes.

Acknowledgements

Author details

Yun-Chih Chiang[1] and Sung-Shan Hsiao[2]

1 Tzu Chi University, Taiwan

2 National Taiwan Ocean University, Taiwan

References

[1] Almar, R, Castelle, B, Ruessink, B. G, Sénéchal, N, Bonneton, P, & Marieu, V. (2010). Two- and three-dimensional double-sandbar system behaviour under intense wave forcing and a meso-macro tidal range", Continental Shelf Research, , 30, 781-792.

[2] Briand, M, & Kamphuis, J. W. (1993). Waves and currents on natural beaches: a quasi 3d numerical model," *Coastal Eng.* 20, , 101-134.

[3] Brøker, I, & Stive, M. J. F. (1991). *Validation of hydrological models, phase 1*, Danish Hydraulic Institute, Horsholm, Denmark.

[4] Brøker, I, Deigaard, R, & Fredsøe, J. (1991). Onroffshore sediment transport and morphological modelling of coastal profiles," *Proc. ASCE Specialty Conf. Coastal Sediments*' 91, Seattle, WA, , 643-657.

[5] Chiang, Y. C, Hsiao, S. S, & Lin, M. C. D Sediment Transport Modeling for Coastal Morphodynamics", Proc. of the 21 (2011) International Offshore and Polar Eng. Conference, Maui, Hawaii, USA, June 19-24, , 1053-1058.

[6] Cox, D, & Kobayashi, N. (1996). Undertow profiles in the bottom boundary layer under breaking waves." 25th *Int. Conf. Coastal Eng.*, ASCE , 3, 3194-3206.

[7] Davies, A, & Thorne, P. (2002). DV modelling of sand transport by waves and currents in the rippled bed regime," In: *Coastal Eng. Conf.* 2002 (ICCE). ASCE, New York, , 2600-2611.

[8] Davis, A. G, & Villaret, C. (2003). Sediment Transport Modelling for Coastal Morphodynamics," *Proc. of the International Conference on Coastal Sediments*, 2003, Florida, USA, , 1-14.

[9]   Deigaard, D, Fredsøe, J, & Hedegaard, I. B. (1986). Suspended sediment in the surf zone," *J. of Waterway, Port, Coastal and Ocean Eng.*, ASCE, , 112, 115-128.

[10] Deigaard, R, & Fredsøe, J. (1989). Shear stress distribution in dissipative water waves," *Coastal Eng.*, , 13, 357-378.

[11] Deigaard, R, Justesen, P, & Fredsøe, J. (1991). Modelling of undertow by a one-equation turbulence model." *Coastal Eng.*, , 15, 431-458.

[12] Deigaard, R. (1993). A note on the three-dimensional shear stress distribution in a surf zone." *Coastal Eng.* , 20, 157-171.

[13] De Vriend, H. J, & Stive, M. J. F. (1987). Quasi-3D Modelling of Nearshore Currents," *Coastal Eng.*, , 11, 565-600.

[14] Dibajnia, M, & Watanabe, A. (1996). A transport rate formula for mixed-size sands," P*roc. 25th Int. Conf. on Coastal Eng.*, , 3791-3804.

[15] Dibajnia, M, & Watanabe, A. (1998). Transport rate under irregular sheet flow conditions," *Coastal Eng.* , 35, 167-183.

[16] Dibajnia, M, & Kioka, W. (2000). Long waves and the change in cross-shore sediment transport rates on a sheet flow dominated beach," *Coastal Eng. Jpn.*, JSCE & World Scientific, , 42-1, 87-110.

[17] Dibajnia, M, & Watanabe, A. (2001). A representative wave model for estimation of nearshore local transport rate," *Coastal Eng. Jpn.* , 43, 1-38.

[18] Drønen, N, & Deigaard, R. (2000). Three dimensional near-shore bar morphology." *Proc. 27th Int. Conf. on Coastal Eng.* ASCE, Sydney, , 3205-3217.

[19] Drønen, N, & Deiggard, R. (2007). Quasi-three-dimensional modelling of the morphology of longshore bars," *Coastal Eng.* , 54, 197-215.

[20] Elfrink, B, Broker, I, Deigaard, D, Hansen, E, & Justesen, P. (1996). Modelling of q3d sediment transport in the surf zone," In: Edge, B.L. (Ed.), *Coastal Eng. Conf.* ASCE, Orlando, Florida, USA, , 3805-3817.

[21] Elgar, S. (1987). Relationships involving third moments and bispectra of a harmonic process," *IEEE Trans. on Acoustics, Speech, and Signal Processing,* 35, , 1725-1726.

[22] Elgar, S, Guza, R. T, & Freilich, M. H. (1988). Eulerian measurements of horizontal accelerations in shoaling gravity waves," *J. Geophys. Res.*, , 93, 9261-9269.

[23] Elgar, S, Gallagher, E. L, & Guza, R. T. (2001). Nearshore sandbar migration," *J. of Geophysical Research*, , 106(C6), 11623-11627.

[24] Fernando, P. T, & Pan, S. (2005). Modelling wave of hydrodynamics around a scheme of detached leaky breakwaters," In: Smith, J.M. (Ed.), *Proceeding of the 29th International Conference on Coastal Eng..* World Scientific, Lisbon, Portugal, , 830-841.

[25] Fredsøe, J, & Deigaard, R. (1992). *Mechanics of Coastal Sediment Transport*, World Scientific, Singapore.

[26] Hoefel, F, & Elgar, S. (2003). Wave-induced sediment transport and sandbar migration", Science, , 299, 1885-1887.

[27] Houser, C, & Greenwood, B. (2007). Onshore Migration of a Swash Bar During a Storm", J. of Coastal Research, , 23, 1-14.

[28] Hsu, T, Elgar, J, Guza, S, & Wave-induced, R. T. sediment transport and onshore sandbar migration", Coastal Eng., , 53, 817-824.

[29] Kuroiwa, M, Noda, H, & Matsubara, Y. (1998). Applicability of a quasi-three dimensional numerical model to nearshore currents," *Proc. of 26th ICCE*, , 815-828.

[30] Kennedy, A. B, Chen, Q, Kirby, J. T, & Dalrymple, R. A. (2000). Boussinesq Modeling of Wave Transformation, Breaking, and Runup. I: 1D," *Journal of Waterway, Port, Coastal and Ocean Eng.*, ASCE, , 126(1), 39-47.

[31] Li, M, Fernando, P. T, Pan, S, Connor, O, & Chen, B. A. D., ((2007). Development of a quasi-3d numerical model for sediment transport prediction in the coastal region." *Journal of Hydro-environment Research*, , 1, 143-156.

[32] Lin, M. C, Kuo, J. C, Chiang, Y. C, & Liou, J. Y. (1996). Numerical Modeling of Topography Changes in Sea Region," *Proc. 18th Conf. on Ocean Engineering in Republic of China*, Nov. 1996, , 627-637.

[33] Lin, M. C, Chiang, Y. C, & Hsiao, S. S. (2009). A study of the sediment transport formula under combined wave and current conditions." *J. of Coastal and Ocean Eng.*, , 9(2), 177-205.

[34] Long, W, Kirby, J. T, & Hsu, T. J. ((2006). Cross shore sandbar migration predicted by a time domain Boussinesq model incorporating undertow", *Coastal Eng*. Conf., , 2655-2667.

[35] Nielsen, P. (1992). *Coastal Bottom Boundary Layers and Sediment Transport*, Advanced Series on Ocean Engineering. Singapore: World Scientific Publication., 4

[36] Nwogu, O. (1993). An Alternative Form of the Boussinesq Equations for Modeling the Propagation of Waves from Deep to Shallow Water," *J. of Waterway, Port, Coastal and Ocean Eng.*, ASCE, , 119(6), 618-638.

[37] Okayasu, A, Shibayama, T, & Horikawa, K. (1988). Vertical variation of undertow in the surf zone," *Proc. 21st Int. Conf. on Coastal Eng.*, ASCE, Malaga, , 478-491.

[38] Okayasu, A, & Katayama, H. (1992). Distribution of undertow and long-wave component velocity due to random waves," *Proc. of 23rd Int. Conf. on Coastal Eng.*, ASCE, , 883-893.

[39] Okayasu, A, Hara, K, & Shibayama, T. (1994). Laboratory experiments on 3-D nearshore currents and a model with momentum flux by breaking wave," *Proc. 24th Int. Conf. Coastal Eng.*, , 2461-2475.

[40] Pape, L, Plant, N. G, & Ruessink, B. G. (2010). On cross-shore migration and equilibrium states of nearshore sandbars," *J. of Geophysical Research*, , 115, 1-15.

[41] Rakha, K. A. d phase resolving hydrodynamic and sediment transport model." *Coastal Eng.* , 34, 277-311.

[42] Roelvink, J. A, & Reniers, A. J. H. M. (1995). LipllD Delta Flume Experiments, a profile dataset for profile model validation. Report H2130, January 1995, Delft Hydraulics, The Netherlands.

[43] Ruessink, B. G, Kuriyama, Y, Reniers, A. J. H. M, Roelvink, J. A, & Walstra, D. J. R. (2007). Modeling cross- shore sandbar behavior on the timescale of weeks", *J. Geophys. Res.*, 112, F03010.

[44] Ruessink, B. G, & Kuriyama, Y. (2008). Numerical predictability experiments of cross-shore sandbar migration", *Geo. Research Letters*, , 35, 16-35.

[45] Ruessink, B. G, Pape, L, & Turner, I. L. (2009). Daily to interannual cross-shore sandbar migration: Observations from a multiple sandbar system", *Continental Shelf Research*, , 29, 1663-1677.

[46] Sanchez-arcilla, A, Collado, F, & Rodriguez, A. (1992). Vertically varying velocity field in Q-3D nearshore circulation," *Proc. of Int. Coastal Eng. Conference*, , 2811-2824.

[47] Soulsby, R. L. (1997). Dynamics of marine sands, Thomas Telford Publications, London.

[48] Soulsby, R. L, Hamm, L, Klopman, G, Myrhaug, D, Simons, R, & Thomas, G. (1993). Wave-current interaction within and outside the bottom boundary layer," *Coastal Eng.* , 21, 41-69.

[49] Splinter, K. D, Holman, R. A, & Plant, N. G. dynamic model for sandbar migration and 2DH evolution", J. of Geophysical Research, , 116, 10-20.

[50] Svendsen, I. A. (1984). Wave heights and set-up in a surf zone." *Coastal Eng.* , 8, 303-329.

[51] Svendsen, I. A, & Lorenz, R. S. (1989). Velocities in combined undertow and longshore currents," *Coastal Eng.*, , 13, 55-79.

[52] Ting, F. C. K, & Kirby, J. T. (1994). Observation of undertow and turbulence in a laboratory surf zone." *Coastal Eng.* , 24, 51-80.

[53] Trowbridge, J, & Madsen, O. S. (1984). Turbulent Wave Boundary Layers 1. Model Formulation and First- Order Solution," *J. Geophys. Res.*, C5), , 89, 7989-7997.

[54] Trowbridge, J, & Young, D. (1989). Sand transport by unbroken waves under sheet flow conditions," *J. Geophys. Res.*, , 94, 10.

[55] Wai, O, Chen, Y, & Li, Y. driven coastal sediment transport model." *Coastal Eng. Journal*, , 46, 385-424.

[56] Wei, G, Kirby, J. T, Grilli, S. T, & Subramanya, R. (1995). A Fully Nonlinear Boussinesq Model for Surface Waves. Part 1. Highly Nonlinear Unsteady Waves," *J. Fluid Mech.*, , 294, 71-92.

[57] Wilson, K. C. (1989). Friction of wave induced sheet flow," *Coastal Eng.* , 12, 371-379.